THE JOURNAL OF PHYSICAL CHEMISTRY B

ARTICLE

pubs.acs.org/JPCB

Molecular Dynamics Simulations of Membranes Composed of Glycolipids and Phospholipids

Jon Kapla, Baltzar Stevensson, Martin Dahlberg, and Arnold Maliniak*

Department of Materials and Environmental Chemistry, Division of Physical Chemistry, Arrhenius Laboratory, Stockholm University, SE-106 91 Stockholm, Sweden

ABSTRACT: Lipid membranes composed of 1,2-di-(9Z,12Z,15Z)-octadecatrienoyl-3-*O*-β-D-galactosyl-*sn*-glycerol or monogalactosyldiacylglycerol (MGDG) and 1,2-dimyristoyl-*sn*-glycero-3-phosphocholine (DMPC) were studied by means of molecular dynamics (MD) computer simulations. Three lipid compositions were considered: 0%, 20%, and 45% MGDG (by mole) denoted as MG-0, MG-20, and MG-45, respectively. The article is focused on the calculation of NMR dipolar interactions, which were confronted with previously reported experimental couplings. Dynamical processes and orientational distributions relevant for the averaging of dipolar interactions were evaluated. Furthermore, several parameters important for characterization of the bilayer structure, molecular organization, and dynamics were investigated. In general, only a minor change in DMPC properties was observed upon the increased MGDG/DMPC ratio, whereas properties related to MGDG undergo a more pronounced change. This effect was ascribed to the fact that DMPC is a bilayer (L_α) forming lipid, whereas MGDG prefers a reverse hexagonal (H_{II}) arrangement.

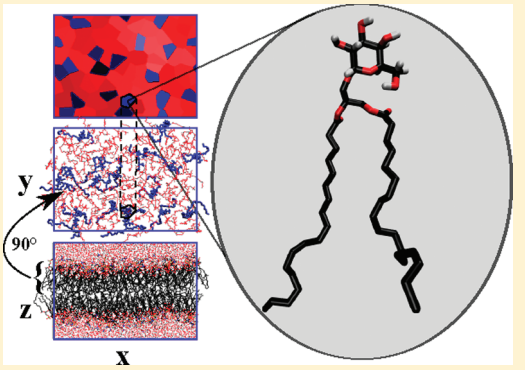

1. INTRODUCTION

A fundamental understanding of structure−function relations of biomembranes relies on detailed information about properties of a lipid bilayer, which is the structural foundation of the membrane. Glycolipids are important structural components of the thylakoid membrane which, in turn, is present in all higher plants and is an essential part of the photosynthetic process.[1] About 50% of the dry weight of this membrane consists of 1,2-di-(9Z,12Z,15Z)-octadecatrienoyl-3-*O*-β-D-galactosyl-*sn*-glycerol or monogalactosyldiacyl-glycerol[2,3] (MGDG, see Figure 1), which makes MGDG the most abundant polar lipid in nature.

Detailed investigations of the photosystem I (PSI) complex using X-ray diffraction showed that MGDG is located close to the core of PSI.[4] This observation suggested that MGDG may be related to the photosynthesis. Additional evidence for the importance of this glycolipid in the photosynthesis was inferred from an investigation in which a mutant with defective MGDG synthase developed severe defects in the chloroplast structure and a reduction in chlorophyll content.[5] The presence of MGDG is considered crucial for protein folding and insertion, as well as for translocation of proteins across membranes.[3] Several studies have focused on the biochemical aspects of this glycolipid, but the knowledge at the molecular level is still limited regarding the structure and dynamics of MGDG inserted into membranes.[6−10] In the present article bilayers formed by MGDG and 1,2-ditetradecanoyl-*sn*-glycero-3-phosphocholine or 1,2-dimyristoyl-*sn*-glycero-3-phosphocholine (DMPC, Figure 1) were investigated using molecular dynamics (MD) computer simulations.

Clearly, many of the characteristics of MGDG are closely related to its molecular structure. The fact that MGDG has a small galactose headgroup, in comparison to its unsaturated chains, results in a high value of the packing parameter,[11,12] defined as v/la_0 where v is the volume of the hydrophobic part of the lipid, l is the length of hydrocarbon chains, and a_0 is the area per headgroup. Hydrated MGDG forms therefore a reversed (type-II) hexagonal liquid crystalline (H_{II}) phase.[11,13] However, when this glycolipid is incorporated into a phospholipid matrix, lamellar structures such as the L_α phase can be obtained.[6] Thus, mixtures of MGDG and a bilayer-forming lipid, such as DMPC, exhibit lamellar, hexagonal, and probably cubic phases.[9] It is interesting to note that the presence of both nonbilayer-forming and bilayer-forming lipids in biological membranes seems to be important for several biochemical phenomena.[14]

The rapid development of computer power has enabled molecular modeling of increasingly more complex chemical systems. Molecular dynamics computer simulations of one- and multicomponent lipid systems using both atom-scale and coarse-grained interaction models have attracted considerable attention in the scientific literature.[15−23] In particular several mixtures of lipids with different acyl chain lengths and degrees of saturation have been reported.[24−28] In several of these simulations cholesterol has been included, which may trigger lipid segregation phenomena and coexistence of ordered-disordered domains. Modeling studies of glycolipids incorporated into bilayers are, however, still very scarce.[29−32]

Recently we have employed various NMR techniques for investigations of MGDG/DMPC mixtures.[33] In particular, we used

Received: September 26, 2011
Revised: November 21, 2011
Published: November 28, 2011

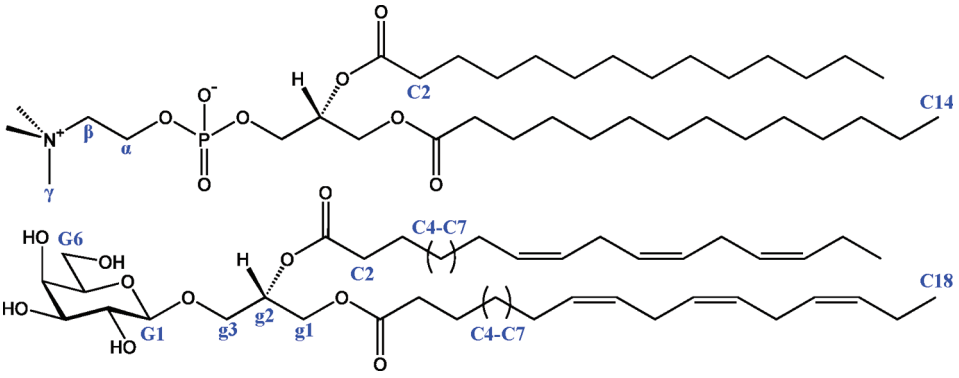

Figure 1. Schematic structures of 1,2-dimyristoyl-*sn*-glycero-3-phosphocholine (DMPC, top) and 1,2-di-(9*Z*,12*Z*,15*Z*)-octadecatrienoyl-3-*O*-β-D-galactosyl-*sn*-glycerol or monogalactosyldiacylglycerol (MGDG, bottom). Note that the glycerol hydrogens are not interaction sites; these are merely included in the figure to indicate the chiral centers of the lipids.

^{31}P NMR for verification of the phase diagram and determined ^{1}H−^{13}C dipolar couplings in the lamellar (L_α) phase. The measurement of dipolar interactions[34−38] is an attractive technique to investigate fluid phase lipids and does not, in contrast to deuterium NMR, require isotopic enrichment or tedious sample preparation. Dipolar interactions provide information on the local orientational order and molecular conformations. In analogy with quadrupolar interactions determined by deuterium NMR, experimental dipolar couplings provide only the magnitude of the interaction, but not the sign. This sign can however be readily determined from computer modeling, which is a powerful complement to experimental NMR studies of model biomembranes. In the present study we perform atomic-scale MD simulations of fully hydrated lipid bilayers with three different compositions of MGDG and DMPC lipids: 0%, 20%, and 45% MGDG by mole. In the following we will denote these systems as MG-0, MG-20, and MG-45, where MG-0 corresponds to a pure DMPC membrane.

2. SYSTEMS AND METHODS

The mixed bilayers were prepared by periodically replicating small equilibrated bilayer patches to the desired size and concentration. The MG-20 system was built with 36 MGDG and 144 DMPC lipids (total 180), whereas MG-45 consisted of 80 MGDG and 96 DMPC (total 176). The bilayers were solvated by 25 water molecules per lipid to a total of 4500 and 4400 water molecules for MG-20 and MG-45, respectively. The reference system MG-0 consisted of 128 DMPC lipids and 3200 water molecules. The systems were energy-minimized with a steepest descent algorithm until converged before they were used in any further simulations.

The DMPC topology is freely available online from the Web site of the Biocomputing group at the University of Calgary.[28] The topology for the MGDG lipid was created by bridging a galactose ring (the structure obtained from the Avogadro Software[39]) to a lipid backbone with a (G1 → g3) glycosidic linkage. The united atom model for lipids reported by Berger et al.[40] was combined with the optimized potentials for liquid simulations, all-atom (OPLS-AA) force field[41] using the half-ε, double pairlist method[42] as reported by Neale et al. This method is used to ensure proper scaling of the 1−4 Lennard−Jones parameters from the Berger force field when combining it with OPLS-AA, using the Groningen machine for chemical simulations (GROMACS) simulation package. In principle, an invisible border in treatment of the interactions in the lipid can be imagined between atoms Og3 and Cg3 of MGDG in Figure 1. The galactose interaction parameters for OPLS-AA were taken from ref 43. On the basis of a comparison of parameters for similar atoms in both force fields, the charges of Cg3 and Cg2 were slightly modified, from 0.4 to 0.5 and 0.3 to 0.4, respectively. This assures the charge neutrality and a better compatibility with the OPLS-AA interaction scheme.

The glycosidic linkage in MGDG was modeled using Ryckert−Belleman dihedrals[44] converted from Damm et al.,[45] but for the dihedrals Og3−Cg3−Cg2−Cg1 and Og3−Cg3−Cg2−Og2 the Berger parameters were used. The 1−4 Lennard−Jones interactions related to the glycosidic linkage and involving atoms from both parameter sets were scaled using two different procedures: for Cg2−CG1, Cg3−CG2, and Cg3−OG5 the scaling according to the OPLS-AA model was used, whereas a scaling based on the half-ε, double pairlist method was applied to Cg1−Og3 and Og2−Og3. This ensures the 1−4 interactions to be properly scaled and compatible with the corresponding bonded interactions. The angle bending was modeled using generic OPLS-AA and Berger parameters for angles CG1−Og3−Cg3 and Og3−Cg3−Cg2, respectively. Berger parametrs were also used to model the Cg3−Og3 bond stretching. The six double bonds were modeled employing parameters originally used by Bachar et al.[46] for the modeling of 1-palmitoyl-2-linoleyl-*sn*-glycero-3-phosphatidylcholine (PLPC).

Preliminary tests of 100 ns simulations were carried out for MG-20 and MG-45 using TIP3P[47] and simple point-charge (SPC)[48] water models, revealing that the bilayer properties were essentially independent of the water model. Therefore only the SPC water results are reported.

All simulations were carried out in the NPT ensemble using the GROMACS v4.0.7 software package.[49] The temperature and pressure were controlled by using the Berendsen thermostat and semianisotropic barostat[50] with relaxation times of 1 and 5 ps, respectively. The temperature was set to 313 K and the pressure to 1 bar. The electrostatic interactions were calculated explicitly up to a cutoff distance of 1.0 nm, above which the interactions were treated using the particle-mesh Ewald (PME) summation algorithm.[51] The nonbonded interactions were calculated within a cutoff distance of 1.0 nm employing dispersion correction. The center of mass movement was removed in a linear fashion every time step individually for the upper and lower parts of the bilayer and the solvent. All bonds in water and lipids were constrained

dx.doi.org/10.1021/jp209268p |*J. Phys. Chem. B* 2012, 116, 244–252

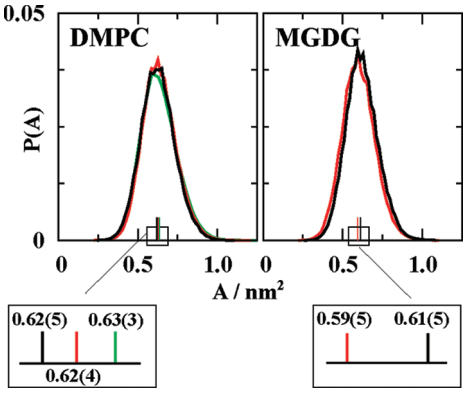

Figure 2. Normalized probability distributions for area per lipid, $P(A)$, calculated for MG-0 (green), MG-20 (red), and MG-45 (black) systems. The average values (standard deviations of the last digit in parentheses) are indicated below the distributions.

using the SETTLE[52] and LINCS algorithms,[53,54] respectively, and the simulations were performed using the leapfrog algorithm with a time step of 2 fs under periodic boundary conditions in rectangular boxes.

All of the systems were equilibrated for 100 ns, followed by the production simulation that lasted for 120, 320, and 260 ns for MG-0, MG-20, and MG-45, respectively.

3. RESULTS AND DISCUSSION

Membrane Properties. The area per lipid is an important parameter frequently used to characterize bilayers and to monitor phase transitions. In homogeneous (one-component) membranes the average area per lipid is readily obtained from the lateral area (*xy*-plane) divided by the number of lipids in a monolayer. The situation is more complicated in multicomponent bilayers where the area per lipid is different for every component. Several approaches for the calculation of the area per lipid have been suggested,[55−57] which were summarized in a *canonical* method based on the concept of partial-specific area.[16] In the present study only three compositions are available, and therefore a simpler, grid-based method[58] was employed. In practice, a two-dimensional (2D) grid of 250 × 250 points was created over a bilayer leaflet, and each lipid was assigned a number of grid points. This was carried out using the center of mass of the lipids and a nearest neighbor procedure. The grid points in the *xy*-plane form polygons, corresponding to a 1:1 mapping: each polygon represents a specific lipid. Preliminary tests of the grid size showed a relatively fast convergence of the area per lipid with increasing grid sizes. Even though the area converged at a grid size of 100 × 100 points, a size of at least 200 × 200 is necessary[58] for the points to form one single polygon per molecule. On the basis of these results we use 250 × 250 grid points for our calculations.

The number of grid points within a polygon gives an estimation of the area per lipid. In Figure 2 the area per lipid distributions are displayed for both lipids in MG-0, MG-20, and MG-45 systems. The average values indicated below the distributions show that, upon increased MGDG concentration, the area per lipid increases for MGDG and decreases for DMPC. These trends are consistent with the fact that MGDG lipids do not form (due to the high packing parameter) lamellar phases, but rather organize into reverse hexagonal structures.[13] The experimental area per

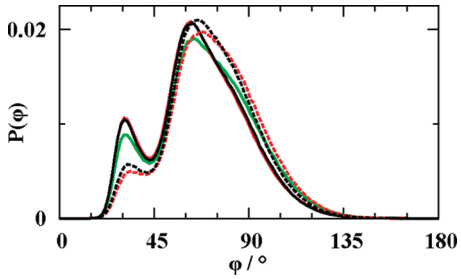

Figure 3. Normalized probability distributions, $P(\varphi)$, for the angle φ, defined as $C8_1-g2-C8_2$, where $C8_n$ is an atom in the nth acyl chain (n = 1, 2). The distributions correspond to DMPC (solid lines) and MGDG (dashed lines) in the MG-0 (green), MG-20 (red), and MG-45 (black) systems.

lipid in a monolayer of MGDG was determined[9] to 0.82 nm^2. To examine the stability of the grid-based method, we have calculated the area per lipid in MG-0 using the standard procedure (area of a leaflet divided by the number of DMPC lipids) and obtained 0.63 ± 0.01 nm^2, where the standard deviation reflects the fluctuations of the box. This value is consistent with the grid approach (0.63 ± 0.03 nm^2). The distributions in Figure 2 are rather broad, which is reflected in the area fluctuations associated with the averages. The main contribution to these fluctuations is the projection procedure of the polygons (with different *z*-components) on a common grid plane. The experimental values for the surface area of DMPC membranes range from 0.60 to 0.67 nm^2 depending on the exact temperature and hydration level of the bilayer.[59−61] Previous MD simulations of DMPC bilayers at 30 °C with 23 water molecules per lipid resulted in an area of 0.604 nm^2,[62] whereas the hydration level of 29 water molecules resulted in 0.631 and 0.654 nm^2 at 30 and 50 °C, respectively.[63]

A molecular geometry parameter that can be related to the area per lipid is the acyl chain angle φ defined by $C8_1-g2-C8_2$, where g2 is the glycerol carbon and $C8_n$ is an atom in the nth acyl chain (n = 1,2). The probability distributions, $P(\varphi)$, for MG-0, MG-20, and MG-45 are displayed in Figure 3. All of the distributions exhibit a pronounced local maximum that has previously been observed in coarse-grained simulations of cardiolipin[64] and attributed to the energy minimum in the Lennard−Jones interaction between the methyl groups in the acyl chains. For DMPC the distribution becomes more narrow upon insertion of MGDG (i.e., MG-0 to MG-20) but does not undergo further change in MG-45. For MGDG the distribution is broader in MG-20, indicating higher order in the MG-45 system.

The membrane thickness is closely associated with the area per lipid and reflects the lipid volume. The distributions of the *z*-component for the interlipid headgroup distances are displayed in Figure 4: phosphate−phosphate in DMPC and galactose−galactose in MGDG (defined by the center of mass). Clearly the distributions, in addition to a shift, exhibit different widths, which can be associated with the order in the bilayer. The distributions become more narrow upon increased MGDG concentration, which reflects increased order and rigidity. The membrane becomes thicker upon increased MGDG, which is consistent with the fact that the MGDG lipids consist of two 18-carbon acyl chains, whereas the chains in DMPC contain only 14 carbons. The first maximum in the phosphorus/galactose distributions (at r = 0) corresponds to the lipids located in the same layer. The second maximum can be used as an estimate of the membrane thickness, which for the distributions displayed in Figure 4

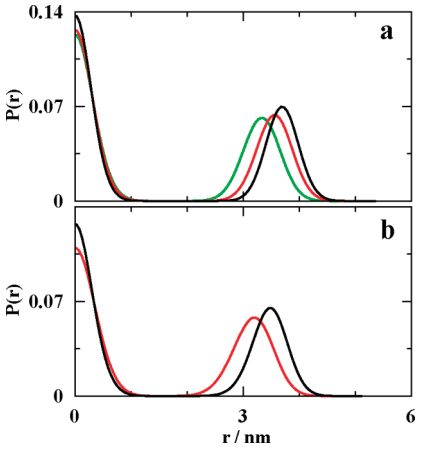

Figure 4. Normalized distributions of distances between phosphorus atoms in DMPC (a) and center of mass in the galactose fragment of MGDG (b). The distributions are labeled: MG-0 (green), MG-20 (red), and MG-45 (black).

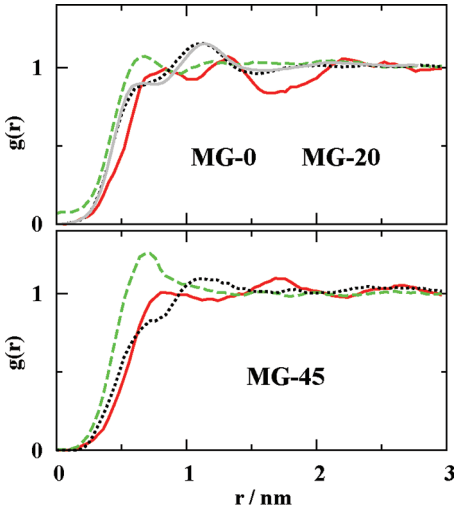

Figure 5. Two-dimensional (*xy*-plane) radial distribution functions (RDFs) calculated for center of mass of the lipids within the same monolayer and averaged over both layers: MGDG−MGDG (solid, red), MGDG−DMPC (dashed, green), and DMPC−DMPC (dotted, black). The DMPC−DMPC distribution in MG-0 is included (solid, gray).

corresponds to: 3.33, 3.56/3.20, and 3.69/3.48 nm for MG-0, MG-20, and MG-45, respectively. The experimental values of the DMPC bilayer thickness, defined as the average distance between phosphate groups on opposite monolayers, are 3.5−3.6 nm[59,65,66] which is in reasonable agreement with our results and previous MD simulations of fully hydrated (29 water molecules/lipid) DMPC bilayers.[63]

Radial Distributions and Lateral Diffusion of Lipids. Two-dimensional (*xy*-plane) radial distributions for the centers of mass of the two lipids are displayed in Figure 5. These distributions describe the average distance dependent probability of finding lipid neighbors, which in turn reflects local deviation from the bulk density. All of the distributions shown in Figure 5 indicate weak preferential positional ordering, and no tendency for lipid segregation is observed. The DMPC−DMPC distribution in MG-0 is identical to those in MG-20 and MG-45. In fact,

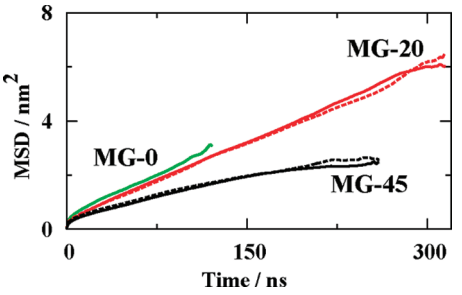

Figure 6. Mean square displacement (MSD) calculated for the center of mass of the lipids: MGDG (dashed) and DMPC (solid).

Table 1. Calculated Lateral Diffusion Coefficients (in $\mu m^2\ s^{-1}$) for the Two Lipids[a]

lipid	MG-0	MG-20	MG-45
MGDG		4.5 ± 0.4	2.5 ± 0.8
DMPC	5.0 ± 0.1	4.7 ± 0.2	2.6 ± 0.5

[a] The indicated errors reflect the deviation of the slopes estimated from the first and second half of the MSD curves in Figure 6.

the RDFs are similar to what would be expected for a densely packed two-dimensional liquid. Similar results were obtained in a combined study of DMPC using MD simulations, X-ray, and neutron scattering experiments.[67]

The lateral translational-diffusion coefficient D_{lat} can be estimated for a molecule undergoing Brownian motion using the Einstein relation

$$D_{lat} = \lim_{t \to \infty} \frac{1}{4t} \langle (r(t) - r(0))^2 \rangle \quad (1)$$

where $r(t)$ is the position of the particle (center of mass) in the *xy*-plane, and the quantity $\langle (r(t) - r(0))^2 \rangle$ is denoted as the mean-square displacement (MSD). The positions of molecules are related to the monolayer center of mass so to avoid artifacts due to the relative motion of the monolayers.[15,63]

The MSDs for the two lipids are displayed in Figure 6, and the calculated D_{lat} are collected in Table 1. The diffusion coefficients of MGDG and DMPC are surprisingly similar in the two mixtures indicating, again, that no lipid segregation takes place in the two systems. The reduction of diffusion upon increased MGDG/DMPC ratio can probably be correlated to the increased order (vide infra). The diffusion coefficient of DMPC in MG-0 was 5.0 $\mu m^2\ s^{-1}$ which is clearly lower than the experimental values 16 and 9 $\mu m^2\ s^{-1}$ determined using the pulsed-field gradient (PFG) NMR spectroscopy[68] and fluorescence recovery after photobleaching (FRAP),[69] respectively. Our value is however similar to that derived from an MD simulation using the same force field.[63] Employing the PFG-NMR technique, lipid diffusion of 5 $\mu m^2\ s^{-1}$ was obtained in the *Acholeplasma laidlawii* membrane (70−80% glycolipids and 20−30% phospholipids).[70] Thus, assuming that the lipid mixture is an ideal system (crude approximation but to some extent supported by the shapes of the RDFs in Figure 5), the diffusion of MGDG in a glycolipid-rich bilayer can be estimated to 2.2 $\mu m^2\ s^{-1}$, which is in reasonable agreement with our values.

NMR Dipolar Couplings and Orientational Order. The measurement of NMR dipolar couplings is a useful experimental

dx.doi.org/10.1021/jp209268p | *J. Phys. Chem. B* 2012, 116, 244–252

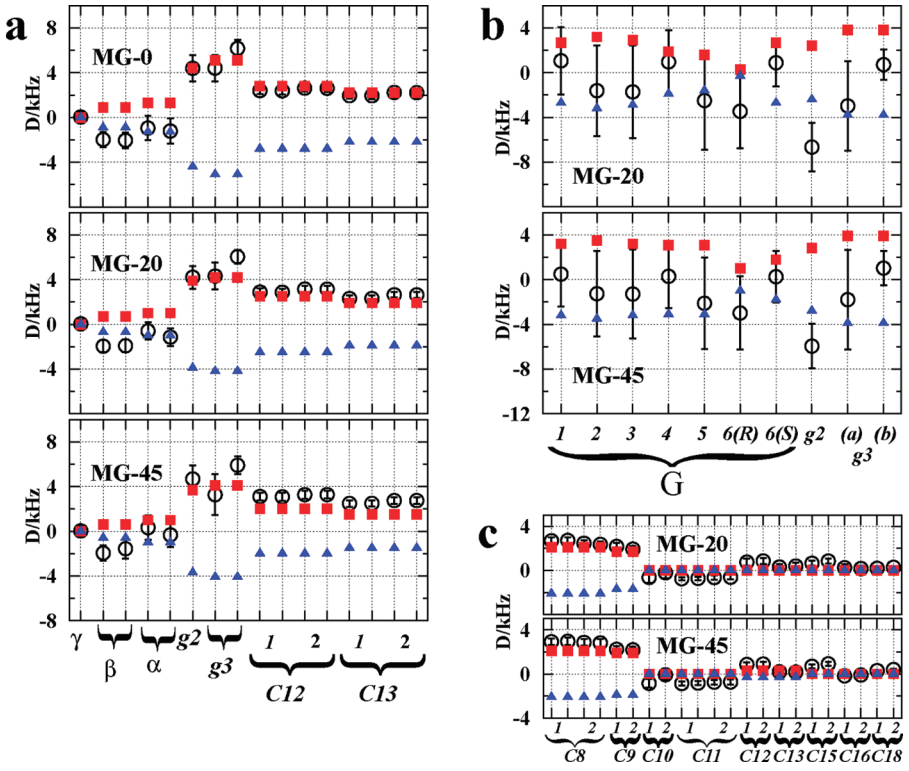

Figure 7. NMR dipolar couplings in DMPC (a), galactose fragment of MGDG (b), and the chains in MGDG (c). The two chains in the lipids are indicated by numbers 1 and 2 (attached to g_1 and g_2), which in turn refer to two couplings in each methylene group. The negative and positive values of the experimental dipolar couplings correspond to triangles (blue) and squares (red), respectively. The calculated values are represented by rings with associated error bars.

method for studies of the molecular structure and local orientational order in soft matter in general and lipid bilayers in particular. All possible dipolar interactions can readily be calculated from a trajectory generated in an MD simulation. Here, we focus on the one -bond $^1H-^{13}C$ couplings that were determined in our experimental study[33] of MGDG/DMPC bilayers. The information contained in these couplings is (in the fast limit of the NMR time scale) identical to the quadrupolar interaction determined from deuterium NMR spectra. The $^1H-^{13}C$ dipolar coupling (in hertz) can be calculated from the MD trajectory using

$$D_{CH} = -\frac{\mu_0}{8\pi^2}\frac{\gamma_C\gamma_H\hbar}{r_{CH}^3}\left\langle\frac{1}{2}(3\cos^2\phi - 1)\right\rangle \quad (2)$$

where ϕ is the angle between the spin−spin vector and the bilayer normal, r_{CH} is the C—H bond length, and the other letters have their usual meaning. The angular bracket denotes an average over all molecular motions and corresponds to S_{CH}, which is the standard order parameter used for characterization of the local order in membranes. We assume that the bilayer normal and the z-axis of the simulation box coincide. The interaction model for the lipids employed in the MD simulations is based on united atoms (except for the galactose unit in MGDG), which means that no hydrogen atoms were included. Instead, the hydrogen positions were calculated from the carbon coordinates. A consequence of not explicitly including protons in the MD simulation is that vibrational contributions to the $^1H-^{13}C$ couplings are to a large extent neglected. Explicit treatment of vibrational corrections in the calculations of dipolar

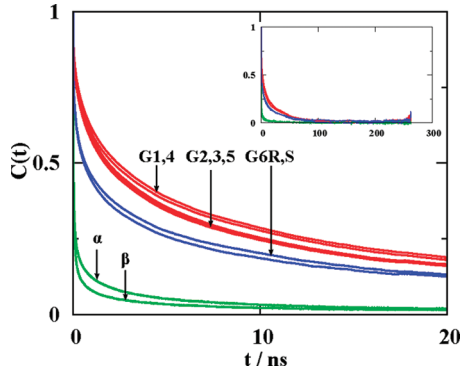

Figure 8. Normalized time correlation functions (TCFs) for the MG-45 system calculated for C—H vectors in MGDG (G1−G6) and in DMPC (α and β). The TCFs with faster decays correspond to G6S and G4. All TCFs calculated over 260 ns are shown in the inset.

couplings have been addressed in several investigations.[71,72] In principle, full quantum chemical calculations are required to correctly estimate this effect. A simpler and frequently employed approach is to use effective (vibrational averaged) bond lengths for calculations of dipolar couplings.[73−75] We have used r_{CH} = 109 pm, which is a commonly accepted value for the vibrational averaged C—H distance in methylene groups. In Figure 7 the experimental and calculated (using eq 2) dipolar couplings are displayed for the different fragments of the two lipids. In analogy with deuterium quadrupolar splittings, the experimental dipolar couplings provide information on the

dx.doi.org/10.1021/jp209268p | J. Phys. Chem. B 2012, 116, 244–252

Table 2. Calculated and Experimental[33] $^{1}H-^{13}C$ Dipolar Couplings (in kHz) in the Galactose Fragment of MGDG

	MG-20		MG-45	
dipolar coupling	calcd	exp.	calcd	exp.
G1	1.1 ± 3.0	2.7	0.5 ± 2.9	3.2
G2	−1.6 ± 4.1	3.2	−1.3 ± 3.8	3.5
G3	−1.7 ± 4.1	2.9	−1.3 ± 4.0	3.2
G4	1.0 ± 2.8	1.9	0.3 ± 2.8	3.1
G5	−2.5 ± 4.4	1.6	−2.1 ± 4.1	3.1
G6R	0.9 ± 2.1	0.3	0.3 ± 2.3	1.0
G6S	−3.5 ± 3.3	2.7	−3.0 ± 3.3	1.8

magnitude, but not on the sign of the interaction. In contrast, both the magnitude and the sign are obtained for the dipolar couplings calculated from the MD trajectory. Thus, the sign of the experimental couplings can be derived for all of the couplings by combination of information contained in experimental and calculated dipolar couplings. The only exception is the galactose moiety in MGDG where the large error bars prevent an unambiguous sign determination. This is so, because the motion of this fragment is considerably slower than other conformational transitions, which restrains a proper averaging. This dynamics can be evaluated by considering the orientational time correlation functions (TCFs) for C—H vectors corresponding to the NMR dipolar interactions. The TCF is defined as[76] $C(t) = \langle D^2_{00}(\Omega(0)) \cdot D^2_{00}(\Omega(t))\rangle$, where $D^2_{00}(\Omega)$ is a second rank Wigner rotation matrix element, and Ω are time-dependent Euler angles relating the orientation of the bilayer normal to a vector fixed in the lipid.

In Figure 8 the TCFs for reorientation of the C—H vectors in the headgroup (G1−G6) of MGDG and α, β in DMPC are displayed for MG-45. The dynamics in MG-20 is very similar (not shown). Qualitatively, the reorientational dynamics becomes slightly slower for MGDG and faster for DMPC with an increased MGDG/DMPC ratio. Furthermore, the dynamics of the galactose is significantly slower compared to the P−N fragment in phosphatidylcholine (PC), which is in agreement with the observation about averaging of the dipolar couplings. Similar results were previously derived[30] from MD simulations of DPPC/glycolipid mixtures. The infinite time limit of TCFs corresponds to $C(\infty) = \langle D^2_{00}(\Omega(0)) \cdot D^2_{00}(\Omega(\infty))\rangle = S^2_{CH}$, where S_{CH} is the orientational order parameter for the vector. For the α and β vectors in DMPC these order parameters are 0.014 and 0.075, which is in agreement with very small values of $C(\infty)$. In Table 2 experimental and calculated dipolar couplings are collected for the galactose unit. We note that all experimental couplings in this fragment are larger for MG-45 compared with MG-20. The only exception is the G6S coupling. Furthermore, the two vectors G6R and G6S exhibit slightly different dynamical behavior (Figure 8), whereas experimental and calculated dipolar couplings differ significantly. In addition, the TCF corresponding to G6S exhibits slightly faster decay, which leads to a smaller error bar compared to G6R (Figure 7b). Therefore, we conclude that this difference is a combination of motional and orientational effects.

The profiles of the local order parameter S_{CH} in acyl chains are shown in Figure 9. Clearly the orientational order for all C—H vectors increases upon addition of MGDG, which has been observed in previous studies.[77,78] This increase is more pronounced in the vicinity of the headgroup in MGDG.

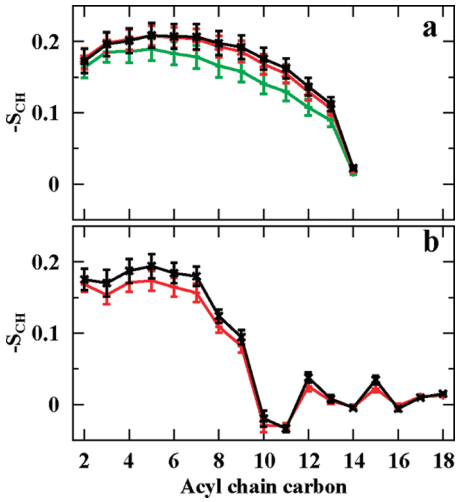

Figure 9. Segmental order parameters, S_{CH} in DMPC (a) and MGDG (b). The different profiles correspond to MG-0 (green), MG-20 (red), and MG-45 (black).

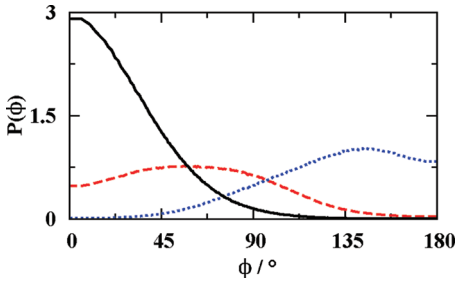

Figure 10. Normalized orientational distribution functions of the vectors related to the C9═C10 bond in MGDG (MG-45/g_2). The distributions of vectors correspond to: C═C (solid, black), C9—H9 (dashed, red), and C10—H10 (dotted, blue).

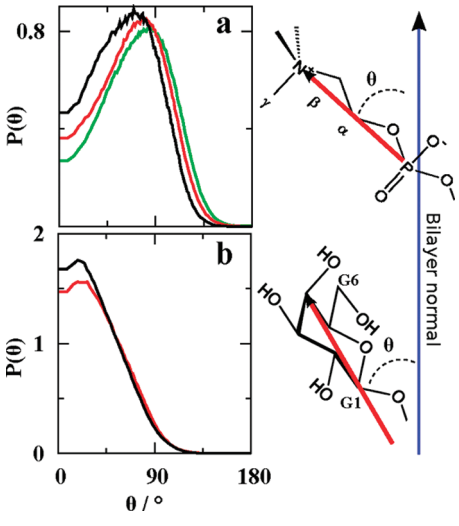

Figure 11. Normalized orientational distribution functions of the P−N vector in DMPC (a) and G1−G4 vector in MGDG (b). The different distributions correspond to MG-0 (green), MG-20 (red), and MG-45 (black).

Dipolar couplings reflect the long-range orientational order and the conformational distributions in the lipids. Therefore, it

dx.doi.org/10.1021/jp209268p | J. Phys. Chem. B 2012, 116, 244–252

is usually not straightforward to provide unambiguous explanations to changes of dipolar couplings caused by alteration of the chemical composition. An interesting effect is experimentally observed at the C10 site of MGDG; although C9 and C10 are located on the same cis double bond, the former interaction is much stronger (Figure 7c) than the latter: 2.2 and −0.1 kHz. Since these segments undergo identical motional averaging, the C9═C10 vector must be tilted with respect to the bilayer normal, thus leaving the C10 average orientation close to the magic angle.[79] This effect was observed both in experimental and calculated dipolar couplings and results in $S_{CH} = 0$ in Figure 7c for C10. Orientational distribution functions for C9═C10 and the two cis C—H vectors are displayed in Figure 10. Indeed, the orientation of the C9═C10 vector is nearly parallel with the director, in agreement with ^{2}H NMR studies[79] of deuterated phospholipids, where this angle was estimated to be 7−9°. The orientation distributions of the two C—H vectors are clearly asymmetric, which is the origin of the different dipolar interactions.

The dipolar couplings for the α, β, and G1−G6-sites reflect the orientation of P−N and G1−G4 vectors in the DMPC and MGDG lipids, respectively. In Figure 11 we display the distribution functions for the orientation of these vectors with respect to the bilayer normal. Note that the detailed information about the orientation of these vectors is lost in the experimental dipolar couplings, simply because the sign of the interaction is not known. The maximum in the P−N vector distributions (Figure 11a) shifts to a lower value; that is, the vector becomes more parallel to the bilayer normal, upon an increased MGDG/DMPC ratio. The average angles were 78.7 ± 6.8°, 75.2 ± 8.3°, and 70.0 ± 1.0° for MG-0, MG-20, and MG-45, respectively. The distributions in Figure 11a result in order parameters, S_{P-N}, of −0.192 ± 0.052, −0.177 ± 0.044, and −0.125 ± 0.070, for MG-0, MG-20, and MG-45, respectively.

The sensitivity of the P−N vector to the charge effects has been previously investigated using computer simulations[80−82] and NMR spectroscopy.[83−85] In these studies it was concluded, assigning the effect to electrostatic interactions that the average angle of the P−N vector decreases upon the addition of salt. Here a similar effect was observed upon the increased ratio MGDG/DMPC. No such shifts were observed in the G1−G4 distributions in Figure 11b, but the order parameter, S_{G1-G4} increases slightly: 0.15 ± 0.11 and 0.19 ± 0.13 for MG-20 and MG-45, respectively. Thus we conclude that the orientational order of the P−N vector decreases, and G1−G4 increases with the increased MGDG/DMPC ratio.

4. SUMMARY AND CONCLUSIONS

We have performed MD computer simulations of hydrated bilayers formed by 1,2-di-(9*Z*,12*Z*,15*Z*)-octadecatrienoyl-3-*O*-β-D-galactosyl-*sn*-glycerol or monogalactosyldiacylglycerol (MGDG) and 1,2-dimyristoyl-*sn*-glycero-3-phosphocholine (DMPC). Three lipid compositions were investigated: 0%, 20%, and 45% (by mole) MGDG denoted as MG-0, MG-20, and MG-45, respectively. Several parameters relevant for the bilayer structure, molecular organization, and dynamics have been determined. The area per lipid of MGDG and DMPC increases and decreases, respectively, upon the increased MGDG/DMPC ratio. This reflects the large packing parameter and small headgroup of MGDG, which in turn results in the reluctance of MGDG to form lamellar phases and rather organize into (reversed) hexagonal structures. The orientation of the headgroup (G1−G4 vector) in MGDG is not affected by increased MGDG concentration, whereas the P−N vector in DMPC becomes increasingly parallel to the bilayer normal. This may result in a more effective packing of DMPC and therefore decreased area per lipid. The experimental area per lipid of MGDG was determined to 0.70 nm^2 for monolayers in an equimolar mixture with digalactosyldiacylglycerol (DGDG). Despite the fact that DGDG contains two galactose fragments in the polar group, its area per lipid is significantly smaller (0.64 nm^2) than that of MGDG.[9,86] This has been attributed to relative orientations of the polar groups and the degree of unsaturation in the chains of the lipids. The MGDG/DGDG system exhibits several similarities to our MGDG/DMPC bilayers: DGDG has a larger headgroup than MGDG and in contrast to MGDG forms preferably lamellar phases. The interparticle (phosphate−phosphate and galactose−galactose) distributions indicate that the bilayer becomes more rigid upon addition of MGDG. The lateral diffusion of the two lipids is very similar and decreases upon increased MGDG/DMPC ratio owing to the higher order in this system. Increased order was similarly observed in cardiolipin/POPC systems,[25] where cardiolipin, in analogy to MGDG, prefers to organize into a reverse hexagonal structure. The two-dimensional (*xy*-plane) radial distribution functions (RDFs) do not indicate any strong specific interactions or lipid segregation phenomena in the mixture, which is consistent with the trend in the lateral diffusion. In general, only a minor change in DMPC properties is observed upon the increased MGDG/DMPC ratio, whereas properties related to MGDG undergo a more pronounced change.

Measurement of NMR C—H dipolar interactions is a powerful method for investigations of molecular structure and local orientational order in lipid bilayers. In analogy with deuterium NMR, experiments provide only the magnitude but not the sign of the interactions. The dipolar couplings derived from a trajectory generated in an MD simulation provide, on the other hand, both the magnitude and the sign of the dipolar coupling. We have calculated C—H dipolar couplings and compared the values with our previous experimental results.[33] The profiles of the local order parameters calculated from the trajectory are consistent with order parameters in single component saturated and unsaturated lipid membranes. Furthermore, we have calculated orientational distributions for the C—H vectors and motional processes relevant for the averaging of some of the couplings. It turned out that the slow reorientation of the galactose headgroup in MGDG restricted proper averaging of the calculated dipolar couplings in this fragment.

AUTHOR INFORMATION

Corresponding Author

*E-mail: arnold.maliniak@mmk.su.se (A.M.).

ACKNOWLEDGMENT

This work was supported by the Swedish Research Council (VR) and the Carl Trygger Foundation.

REFERENCES

(1) Miller, K. R. Structure of A Bacterial Photosynthetic Membrane. *Proc. Natl. Acad. Sci.* **1979**, *76*, 6415–6419.

(2) Gounaris, K.; Barber, J. Monogalactosyldiacylglycerol - the Most Abundant Polar Lipid in Nature. *Trends Biochem. Sci.* **1983**, *8*, 378–381.

(3) Dörmann, P.; Benning, C. Galactolipids rule in seed plants. *Trends Plant Sci.* **2002**, *7*, 112–118.
(4) Jordan, P.; Fromme, P.; Witt, H. T.; Klukas, O.; Saenger, W.; Krauss, N. Three-dimensional structure of cyanobacterial photosystem I at 2.5 angstrom resolution. *Nature* **2001**, *411*, 909–917.
(5) Jarvis, P.; Dörmann, P.; Peto, C. A.; Lutes, J.; Benning, C.; Chory, J. Galactolipid deficiency and abnormal chloroplast development in the Arabidopsis MGD synthase 1 mutant. *Proc. Natl. Acad. Sci.* **2000**, *97*, 8175–8179.
(6) Chupin, V.; Vanthof, R.; Dekruijff, B. The Transit Sequence of a Chloroplast Precursor Protein Reorients the Lipids in Monogalactosyl Diglyceride Containing Bilayers. *FEBS Lett.* **1994**, *350*, 104–108.
(7) Howard, K. P.; Prestegard, J. H. Membrane and solution conformations of monogalactosyldiacylglycerol using NMR/molecular modeling methods. *J. Am. Chem. Soc.* **1995**, *117*, 5031–5040.
(8) Bechinger, B.; Macdonald, P. M.; Seelig, J. Deuterium NMR-Studies of the Interactions of Polyhydroxyl Compounds and of Glycolipids with Lipid Model Membranes. *Biochem. Biophys. Acta* **1988**, *943*, 381–385.
(9) Bottier, C.; Gean, J.; Artzner, F.; Desbat, B.; Pezolet, M.; Renault, A.; Marion, D.; Vie, V. Galactosyl headgroup interactions control the molecular packing of wheat lipids in Lahgmuir films and in hydrated liquid-crystalline mesophases. *Biochim. Biophys. Acta Biomembr.* **2007**, *1768*, 1526–1540.
(10) Lindblom, G.; Orädd, G. Lipid lateral diffusion and membrane heterogeneity. *Biochim. Biophys. Acta Biomembr.* **2009**, *1788*, 234–244.
(11) Evans, D. F.; Wennerström, H. *The Colloidal Domain where Physics, Chemistry, and Biology Meet*, 2nd ed.; Wiley-VCH: New York, 1999.
(12) Israelachvili, J. N.; Mitchell, D. J.; Ninham, B. W. Theory of self-assembly of hydrocarbon amphiphiles into micelles and bilayers. *J. Chem. Soc., Faraday Trans. 2: Mol. Chem. Phys.* **1976**, *72*, 1525–1568.
(13) Shipley, G. G.; Green, J. P.; Nichols, B. W. Phase Behavior of Monogalactosyl, Digalactosyl, and Sulfoquinovosyl Diglycerides. *Biochem. Biophys. Acta* **1973**, *311*, 531–544.
(14) Tsvetkova, N. M.; Horvath, I.; Torok, Z.; Wolkers, W. F.; Balogi, Z.; Shigapova, N.; Crowe, L. M.; Tablin, F.; Vierling, E.; Crowe, J. H.; Vigh, L. Small heat-shock proteins regulate membrane lipid polymorphism. *Proc. Natl. Acad. Sci.* **2002**, *99*, 13504–13509.
(15) Siu, S. W. I.; Vacha, R.; Jungwirth, P.; Böckmann, R. A. Biomolecular simulations of membranes: Physical properties from different force fields. *J. Chem. Phys.* **2008**, *128*, 125103.
(16) Edholm, O.; Nagle, J. F. Areas of molecules in membranes consisting of mixtures. *Biophys. J.* **2005**, *89*, 1827–1832.
(17) Hanasaki, I.; Walther, J. H.; Kawano, S.; Koumoutsakos, P. Coarse-grained molecular dynamics simulations of shear-induced instabilities of lipid bilayer membranes in water. *Phys. Rev. E* **2010**, *82*, 051602.
(18) May, E. R.; Kopelevich, D. I.; Narang, A. Coarse-grained molecular dynamics simulations of phase transitions in mixed lipid systems containing LPA, DOPA, and DOPE lipids. *Biophys. J.* **2008**, *94*, 878–890.
(19) Müller, M.; Katsov, K.; Schick, M. Biological and synthetic membranes: What can be learned from a coarse-grained description? *Phys. Rep.: Rev. Sect. Phys. Lett.* **2006**, *434*, 113–176.
(20) Knecht, V.; Mark, A. E.; Marrink, S. J. Phase behavior of a phospholipid/fatty acid/water mixture studied in atomic detail. *J. Am. Chem. Soc.* **2006**, *128*, 2030–2034.
(21) Gurtovenko, A. A.; Vattulainen, I. Pore formation coupled to ion transport through lipid membranes as induced by transmembrane ionic charge imbalance: Atomistic molecular dynamics study. *J. Am. Chem. Soc.* **2005**, *127*, 17570–17571.
(22) Kasson, P. M.; Kelley, N. W.; Singhal, N.; Vrljic, M.; Brunger, A. T.; Pande, V. S. Ensemble molecular dynamics yields submillisecond kinetics and intermediates of membrane fusion. *Proc. Natl. Acad. Sci.* **2006**, *103*, 11916–11921.
(23) Dahlberg, M.; Maliniak, A. Mechanical Properties of Coarse-Grained Bilayers Formed by Cardiolipin and Zwitterionic Lipids. *J. Chem. Theory Comput.* **2010**, *6*, 1638–1649.
(24) Risselada, H. J.; Marrink, S. J. The molecular face of lipid rafts in model membranes. *Proc. Natl. Acad. Sci.* **2008**, *105*, 17367–17372.
(25) Dahlberg, M.; Maliniak, A. Molecular dynamics simulations of cardiolipin bilayers. *J. Phys. Chem. B* **2008**, *112*, 11655–11663.
(26) Marrink, S. J.; de Vries, A. H.; Tieleman, D. P. Lipids on the move: Simulations of membrane pores, domains, stalks and curves. *Biochem. Biophys. Acta Biomembr.* **2009**, *1788*, 149–168.
(27) de Joannis, J.; Coppock, P. S.; Yin, F. C.; Mori, M.; Zamorano, A.; Kindt, J. T. Atomistic Simulation of Cholesterol Effects on Miscibility of Saturated and Unsaturated Phospholipids: Implications for Liquid-Ordered/Liquid-Disordered Phase Coexistence. *J. Am. Chem. Soc.* **2011**, *133*, 3625–3634.
(28) Biocomputing at the University of Calgary. http://moose.bio.ucalgary.ca, 2011.
(29) Róg, T.; Vattulainen, I.; Karttunen, M. Modeling glycolipids: Take one. *Cell. Mol. Biol. Lett.* **2005**, *10*, 625–630.
(30) Róg, T.; Vattulainen, I.; Bunker, A.; Karttunen, M. Glycolipid membranes through atomistic simulations: Effect of glucose and galactose head groups on lipid bilayer properties. *J. Phys. Chem. B* **2007**, *111*, 10146–10154.
(31) Hall, A.; Róg, T.; Karttunen, M.; Vattulainen, I. Role of Glycolipids in Lipid Rafts: A View through Atomistic Molecular Dynamics Simulations with Galactosylceramide. *J. Phys. Chem. B* **2010**, *114*, 7797–7807.
(32) Lingwood, D.; Binnington, B.; Róg, T.; Vattulainen, I.; Grzybek, M.; Coskun, U.; Lingwood, C. A.; Simons, K. Cholesterol modulates glycolipid conformation and receptor activity. *Nat. Chem. Biol.* **2011**, *7*, 260–262.
(33) Castro, V.; Dvinskikh, S. V.; Widmalm, G.; Sandström, D.; Maliniak, A. NMR studies of membranes composed of glycolipids and phospholipids. *Biochem. Biophys. Acta Biomembr.* **2007**, *1768*, 2432–2437.
(34) Dvinskikh, S. V.; Durr, U. H. N.; Yamamoto, K.; Ramamoorthy, A. High-resolution 2D NMR spectroscopy of bicelles to measure the membrane interaction of ligands. *J. Am. Chem. Soc.* **2007**, *129*, 794–802.
(35) Dvinskikh, S. V.; Yamamoto, K.; Durr, U. H. N.; Ramamoorthy, A. Sensitivity and resolution enhancement in solid-state NMR spectroscopy of bicelles. *J. Magn. Reson.* **2007**, *184*, 228–235.
(36) Dvinskikh, S. V.; Castro, V.; Sandström, D. Efficient solid-state NMR methods for measuring heteronuclear dipolar couplings in unoriented lipid membrane systems. *Phys. Chem. Chem. Phys.* **2005**, *7*, 607–613.
(37) Dvinskikh, S. V.; Castro, V.; Sandström, D. Heating caused by radiofrequency irradiation and sample rotation in ^{13}C magic angle spinning NMR studies of lipid membranes. *Magn. Reson. Chem.* **2004**, *42*, 875–881.
(38) Gross, J. D.; Costa, P. R.; Dubacq, J. P.; Warschawski, D. E.; Lirsac, P. N.; Devaux, P. F.; Griffin, R. G. Multidimensional NMR in Lipid Systems - Coherence Transfer Through J-Couplings Under MAS. *J. Magn. Reson. Ser. B* **1995**, *106*, 187–190.
(39) Avogadro: an open-source molecular builder and visualization tool, Version 0.9.7; http://avogadro.openmolecules.net/, 2008.
(40) Berger, O.; Edholm, O.; Jahnig, F. Molecular dynamics simulations of a fluid bilayer of dipalmitoylphosphatidylcholine at full hydration, constant pressure, and constant temperature. *Biophys. J.* **1997**, *72*, 2002–2013.
(41) Jorgensen, W. L.; Tirado-Rives, J. The OPLS Potential Functions for Proteins. Energy Minimization for Crystals of Cyclic Peptides and Crambin. *J. Am. Chem. Soc.* **1988**, *110*, 1657–1666.
(42) Chakrabarti, N.; Neale, C.; Payandeh, J.; Pai, E. F.; Pomes, R. An Iris-Like Mechanism of Pore Dilation in the CorA Magnesium Transport System. *Biophys. J.* **2010**, *98*, 784–792.
(43) Kony, D.; Damm, W.; Stoll, S.; van Gunsteren, W. F. An improved OPLS-AA force field for carbohydrates. *J. Comput. Chem.* **2002**, *23*, 1416–1429.
(44) Ryckaert, J.-P.; Bellemans, A. Molecular Dynamics of Liquid n-Butane Near Its Boiling Point. *Chem. Phys. Lett.* **1975**, *30*, 123–125.
(45) Damm, W.; Frontera, A.; TiradoRives, J.; Jorgensen, W. L. OPLS all-atom force field for carbohydrates. *J. Comput. Chem.* **1997**, *18*, 1955–1970.
(46) Bachar, M.; Brunelle, P.; Tieleman, D. P.; Rauk, A. Molecular dynamics simulation of a polyunsaturated lipid bilayer susceptible to lipid peroxidation. *J. Phys. Chem. B* **2004**, *108*, 7170–7179.

(47) Jorgensen, W. L.; Chandrasekhar, J.; Madura, J. D.; Impey, R. W.; Klein, M. L. Comparison of Simple Potential Functions for Simulating Liquid Water. *J. Chem. Phys.* **1983**, *79*, 926–935.
(48) Berendsen, H. J. C.; Postma, J. P. M.; van Gunsteren, W. F.; Herman, J. In *Intermolecular Forces*; Pullman, B., Ed.; Reidel: Dordrecht, 1981; pp 331−342.
(49) Hess, B.; Kutzner, C.; van der Spoel, D.; Lindahl, E. GROMACS 4: Algorithms for highly efficient, load-balanced, and scalable molecular simulation. *J. Chem. Theory Comput.* **2008**, *4*, 435–447.
(50) Berendsen, H. J. C.; Postma, J. P. M.; van Gunsteren, W. F.; DiNola, A.; Haak, J. R. Molecular Dynamics with Coupling to an External Bath. *J. Chem. Phys.* **1984**, *81*, 3684–3690.
(51) Essmann, U.; Perera, L.; Berkowitz, M. L.; Darden, T.; Lee, H.; Pedersen, L. G. A Smooth Particle Mesh Ewald Method. *J. Chem. Phys.* **1995**, *103*, 8577–8593.
(52) Miyamoto, S.; Kollman, P. A. Settle - An Analytical Version of the Shake and Rattle Algorithm for Rigid Water Models. *J. Comput. Chem.* **1992**, *13*, 952–962.
(53) Hess, B.; Bekker, H.; Berendsen, H. J. C.; Fraaije, J. G. E. M. LINCS: A linear constraint solver for molecular simulations. *J. Comput. Chem.* **1997**, *18*, 1463–1472.
(54) Hess, B. P-LINCS A parallel linear constraint solver for molecular simulation. *J. Chem. Theory Comput.* **2008**, *4*, 116–122.
(55) Chiu, S. W.; Jakobsson, E.; Mashl, R. J.; Scott, H. L. Cholesterol-induced modifications in lipid bilayers: A simulation study. *Biophys. J.* **2002**, *83*, 1842–1853.
(56) Hofsäß, C.; Lindahl, E.; Edholm, O. Molecular dynamics simulations of phospholipid bilayers with cholesterol. *Biophys. J.* **2003**, *84*, 2192–2206.
(57) Falck, E.; Patra, M.; Karttunen, M.; Hyvönen, M. T.; Vattulainen, I. Lessons of slicing membranes: Interplay of packing, free area, and lateral diffusion in phospholipid/cholesterol bilayers. *Biophys. J.* **2004**, *87*, 1076–1091.
(58) Allen, W. J.; Lemkul, J. A.; Bevan, D. R. GridMAT-MD, A Grid-Based Membrane Analysis Tool for Use With Molecular Dynamics. *J. Comput. Chem.* **2009**, *30*, 1952–1958.
(59) Costigan, S. C.; Booth, P. J.; Templer, R. H. Estimations of lipid bilayer geometry in fluid lamellar phases. *Biochem. Biophys. Acta, Biomembr.* **2000**, *1468*, 41–54.
(60) Petrache, H. I.; Dodd, S. W.; Brown, M. F. Area per lipid and acyl length distributions in fluid phosphatidylcholines determined by H-2 NMR spectroscopy. *Biophys. J.* **2000**, *79*, 3172–3192.
(61) Nagle, J. F.; Tristram-Nagle, S. Structure of lipid bilayers. *Biochim. Biophys. Acta, Rev. Biomembr.* **2000**, *1469*, 159–195.
(62) Wohlert, J.; Edholm, O. Dynamics in atomistic simulations of phospholipid membranes: Nuclear magnetic resonance relaxation rates and lateral diffusion. *J. Chem. Phys.* **2006**, *125*, 204703.
(63) Högberg, C. J.; Lyubartsev, A. P. A molecular dynamics investigation of the influence of hydration and temperature on structural and dynamical properties of a dimyristoylphosphatidylcholine bilayer. *J. Phys. Chem. B* **2006**, *110*, 14326–14336.
(64) Dahlberg, M. Polymorphic phase behavior of cardiolipin derivatives studied by coarse-grained molecular dynamics. *J. Phys. Chem. B* **2007**, *111*, 7194–7200.
(65) Kucerka, N.; Tristram-Nagle, S.; Nagle, J. F. Structure of fully hydrated fluid phase lipid bilayers with monounsaturated chains. *J. Membr. Biol.* **2005**, *208*, 193–202.
(66) Kucerka, N.; Liu, Y. F.; Chu, N. J.; Petrache, H. I.; Tristram-Nagle, S. T.; Nagle, J. F. Structure of fully hydrated fluid phase DMPC and DLPC lipid bilayers using X-ray scattering from oriented multilamellar arrays and from unilamellar vesicles. *Biophys. J.* **2005**, *88*, 2626–2637.
(67) Hub, J. S.; Salditt, T.; Rheinstader, M. C.; de Groot, B. L. Short-range order and collective dynamics of DMPC bilayers: A comparison between molecular dynamics simulations, X-ray, and neutron scattering experiments. *Biophys. J.* **2007**, *93*, 3156–3168.
(68) Orädd, G.; Lindblom, G.; Westerman, P. W. Lateral diffusion of cholesterol and dimyristoylphosphatidylcholine in a lipid bilayer measured by pulsed field gradient NMR spectroscopy. *Biophys. J.* **2002**, *83*, 2702–2704.
(69) Almeida, P. F. F.; Vaz, W. L. C.; Thompson, T. E. Lateral Diffusion in the Liquid-Phases of Dimyristoylphosphatidylcholine Cholesterol Lipid Bilayers - A Free-Volume Analysis. *Biochemistry* **1992**, *31*, 6739–6747.
(70) Lindblom, G.; Orädd, G.; Rilfors, L.; Morein, S. Regulation of lipid composition in Acholeplasma laidlawii and Escherichia coli membranes: NMR studies of lipid lateral diffusion at different growth temperatures. *Biochemistry* **2002**, *41*, 11512–11515.
(71) Emsley, J. W.; Longeri, M.; Merlet, D.; Pileio, G.; Suryaprakash, N. An investigation of the structure and bond rotational potential of some fluorinated ethanes by NMR spectroscopy of solutions in nematic liquid crystalline solvents. *J. Magn. Reson.* **2006**, *180*, 245–255.
(72) Emsley, J. W. Vibrational averaging of residual dipolar couplings: dependence on orientational order. *Liq. Cryst.* **2010**, *37*, 913–921.
(73) Henry, E. R.; Szabo, A. Influence of Vibrational Motion on Solid State Lineshapes and NMR Relaxation. *J. Chem. Phys.* **1985**, *82*, 4753–4761.
(74) Ottiger, M.; Bax, A. Determination of relative N-H-N, N-C′, C-α-C′, and C(α)-H-α effective bond lengths in a protein by NMR in a dilute liquid crystalline phase. *J. Am. Chem. Soc.* **1998**, *120*, 12334–12341.
(75) Blackledge, M. Recent progress in the study of biomolecular structure and dynamics in solution from residual dipolar couplings. *Prog. Nucl. Magn. Reson. Spectrosc.* **2005**, *46*, 23–61.
(76) Zannoni, C.; Guerra, M. Molecular dynamics of a model anisotropic system. *Mol. Phys.* **1981**, *44*, 849–869.
(77) Eriksson, P. O.; Rilfors, L.; Wieslander, Å.; Lundberg, A.; Lindblom, G. Order and Dynamics in Mixtures of Membrane Glucolipids from Acholeplasma-Laidlawii Studied by 2H NMR. *Biochemistry* **1991**, *30*, 4916–4924.
(78) Orädd, G.; Andersson, A. S.; Rilfors, L.; Lindblom, G.; Strandberg, E.; Andrén, P. E. α-Methylene ordering of acyl chains differs in glucolipids and phosphatidylglycerol from Acholeplasma laidlawii membranes: H-2-NMR quadrupole splittings from individual lipids in mixed bilayers. *Biochem. Biophys. Acta, Biomembr.* **2000**, *1468*, 329–344.
(79) Seelig, J.; Waespe-Sarcevic, N. Molecular Order in Cis and Trans Unsaturated Phospholipid Bilayers. *Biochemistry* **1978**, *17*, 3310–3315.
(80) Tieleman, D. P.; Marrink, S. J.; Berendsen, H. J. C. A computer perspective of membranes: molecular dynamics studies of lipid bilayer systems. *Biochim. Biophys. Acta, Rev. Biomembr.* **1997**, *1331*, 235–270.
(81) Böckmann, R. A.; Hac, A.; Heimburg, T.; Grubmüller, H. Effect of sodium chloride on a lipid bilayer. *Biophys. J.* **2003**, *85*, 1647–1655.
(82) Sachs, J. N.; Nanda, H.; Petrache, H. I.; Woolf, T. B. Changes in phosphatidylcholine headgroup tilt and water order induced by monovalent salts: Molecular dynamics simulations. *Biophys. J.* **2004**, *86*, 3772–3782.
(83) Marassi, F. M.; Macdonald, P. M. Response of the Headgroup of Phosphatidylglycerol to Membrane-Surface Charge As Studied by Deuterium and phosporus-31 Nuclear Magnetic Resonance. *Biochemistry* **1991**, *30*, 10558–10566.
(84) Macdonald, P. M.; Leisen, J.; Marassi, F. M. Response of Phosphatidylcholine in the Gel and Liquid-Crystalline States to Membrane-Surface Charges. *Biochemistry* **1991**, *30*, 3558–3566.
(85) Scherer, P. G.; Seelig, J. Electric Charge Effects on Phospholipid Headgroups - Phosphatidylcholine in Mixtures with Cationic and Anionic Amphiphiles. *Biochemistry* **1989**, *28*, 7720–7728.
(86) Gallant, J.; Leblanc, R. M. Purification of Galactolipids by High-Performance Liquid-Chromatography for Monolayer and Langmuir-Blodgett-Film Studies. *J. Chromatogr.* **1991**, *542*, 307–316.